Journal of Materials Chemistry

Cite this: *J. Mater. Chem.*, 2012, **22**, 12107

www.rsc.org/materials

PAPER

Phosphorus–nitrogen dual doped carbon as an effective catalyst for oxygen reduction reaction in acidic media: effects of the amount of P-doping on the physical and electrochemical properties of carbon

Chang Hyuck Choi, Sung Hyeon Park and Seong Ihl Woo*

Received 21st February 2012, Accepted 2nd April 2012
DOI: 10.1039/c2jm31079a

A new strategy for enhancing the oxygen reduction reaction (ORR) activity of carbon-based catalysts in acidic media is proposed and characterized; the strategy consists in modifying the ORR through dual doping of nitrogen and phosphorus into the carbon. The P, N-doped carbon is prepared *via* pyrolysis of a mixture composed of dicyandiamide (DCDA), phosphoric acid, cobalt chloride, and iron chloride at 900 °C under an Ar atmosphere. The P-doping induces an uneven surface with many open edged sites in the carbon morphology and increases the carbon surface area from 108.1 to 578.8 $m^2\ g^{-1}$. The XRD, XPS-C_{1s}, and Raman spectroscopy results reveal that the crystallinity and degree of the sp^2-carbon network decrease and the number of defect sites of the carbon increase as the amount of P-doping increases. All catalysts demonstrated similar proportions of N-doping types regardless of the P-doping amount: pyridinic-N and graphitic-N were dominant phases in the carbon lattice. In the ORR, the onset potential of the prepared catalysts was 0.6 V (*vs.* Ag/AgCl) in 1 M $HClO_4$. The N-doped carbon records −0.69 mA mg^{-1} of mass activity at 0.5 V (*vs.* Ag/AgCl), but additional P-doping results in an increase of activity (−2.88 mA mg^{-1}) that is more than fourfold that produced without the additional P-doping. Moreover, additional P-doping also modifies the ORR pathway, as the N-doped carbon induces more than 10% of H_2O_2; however, the P, N-doped carbon produced below 4% of H_2O_2 during the ORR.

1. Introduction

In order to investigate alternative energies, polymer electrolyte membrane fuel cells (PEMFCs) have been recognized as environmentally friendly and highly efficient electricity generating devices.[1,2] The oxygen reduction reaction (ORR) occurs in a PEMFC cathode and this is important because it limits the performance of PEMFCs due to its slow kinetics; therefore, Pt or its alloys are commonly used as catalysts.[3,4] However, the cost of Pt has increased rapidly as a result of the increased demand and limited quantity available. Thus, low economic competitiveness has prevented the successful commercialization of PEMFCs.

Several alternatives, such as novel metal-based,[5–8] transition metal-based,[9–12] and carbon-based catalysts,[13–16] have been suggested by various research groups during the past decade. Among the candidates, N-doped carbon has recently attracted much attention due to its low price and high stability; however, it has exhibited a low performance in the ORR. Some research groups have reported that the ORR activity of N-doped carbon is comparable to or higher than that of Pt in basic media.[17–21] However, PEMFCs have an acidic environment because Nafion is used as the proton-transfer electrolyte, and N-doped carbon exhibits a much lower ORR activity in acidic media compared with Pt catalysts.

Various advanced techniques have been developed in order to modify the carbon-based catalysts with high ORR activities by providing them with desirable features (*e.g.* large edge fractions, many pyridinic-N sites, large micropore surface area, and highly ordered sp^2-bonding of the carbon structure); these techniques involve secondary pyrolysis of a prepared carbon-based catalyst with an N-containing precursor,[22,23] the use of sacrificial supports such as silica in the pyrolysis step,[23,24] or modification of the carbon pore using a pore filler with small amounts of transition metals followed by a second pyrolysis.[25]

As a new strategy for developing the ORR activity of N-doped carbon, the additional doping of P into N-doped carbon during the growth step of the carbon was attempted in this study. There have been some reports on the dual doping of nitrogen and other heteroatoms into carbon in order to enhance the catalytic activity. Ozaki *et al.* argued that additional doping of B into the N-doped carbon improved the ORR activity through the formation of a new active site, B–N–C.[26] The authors' previous study also revealed that the dual doping of S and N into carbon increased the ORR activity in acidic media.[27] However, the

Department of Chemical and Biomolecular Engineering, Korea Advanced Institute of Science and Technology, Daejeon, 305-701, Republic of Korea. E-mail: siwoo@kaist.ac.kr; Fax: +82-42-350-8890; Tel: +82-42-350-3918

enhancement of the ORR activity for carbon-based catalysts has not yet been studied in detail. Recently, Liu *et al.* demonstrated that P-doped carbon had good ORR activity in basic media.[28] However, P-doped carbon and its related materials have not yet been studied extensively in acidic environments because the electron structure and atomic size of P are dissimilar to those of C; in contrast, those of the commonly used dopants (B and N) are similar to those of C.

In this study, P was doped into N-doped carbon synthesized from dicyandiamide (DCDA) pyrolysis. DCDA is a white powder that is very stable, non-flammable, and cheap; therefore, it is a good precursor for synthesizing N-doped carbon compared with conventionally used chemicals (*e.g.* NH_3, methane, Mephthalocyanine, acetonitrile, *etc.*). DCDA was used as a source of both C and N, and it was carbonized onto $CoCl_2$ and $FeCl_2$ at 900 °C under an Ar atmosphere. Phosphoric acid, which is a common activating agent of carbon,[29–31] was used as the P source. The electrochemical properties of the ORR in acidic media and its physicochemical characteristics were investigated according to the different amounts of P-doping into the N-doped carbon.

2. Experimental

2.1 Synthesis of the P, N-doped carbon

The P, N-doped carbon was prepared *via* the pyrolysis of a homogeneous mixture consisting of DCDA, phosphoric acid, and metal chlorides. Briefly, DCDA (5 g, Aldrich), phosphoric acid (Daejung), $FeCl_2 \cdot 4H_2O$ (3.8 mmol, Yakumi Pure Chemical Co. Ltd.), and $CoCl_2 \cdot 6H_2O$ (9.5 mmol, Aldrich) were dissolved in 100 mL of DI-water *via* stirring for 30 min. The amount of P was controlled by altering the amount of added phosphoric acid: 0, 5, 10, 15, and 20 wt% ratios of phosphoric acid to DCDA were prepared. The solvent was removed using an evaporator (BUCHI R-200) operated at 80 °C and 300 mbar. The gel-like mixture prepared was dried overnight in an oven at 80 °C. After grinding, the powder was loaded on a quartz boat and placed in the middle of a quartz tube reactor. The pyrolysis of the powder was performed at 900 °C for 3 h under 50 cm^3 min^{-1} of Ar flow. The pyrolyzed composite was stirred in 400 mL of aqua regia (Daejung) for 9 h in order to dissolve the Fe and Co particles in the carbon. Finally, the catalysts were filtered, washed with DI-water, and then dried in an oven at 90 °C. The catalysts obtained are abbreviated to NDC, PNDC-5, PNDC-10, PNDC-15, and PNDC-20, where NDC and PNDC indicate the N-doped carbon and P, N-doped carbon, respectively, and the number reflects the amount of phosphoric acid added to the precursor solution in the first step.

2.2 Physical characterizations

The physical properties of the prepared catalysts were examined *via* transmission electron microscopy (TEM), X-ray photoelectron spectroscopy (XPS), element analysis (EA), and inductively coupled plasma (ICP), X-ray diffraction (XRD), Raman spectroscopy, and Brunauer–Emmett–Teller (BET) surface area analyses. The experimental details are as follows. The TEM images were taken at 200 kV with a JEM2100-F (Jeol Ltd) equipped with EDS. The XPS analysis was performed using a Sigma Probe (Thermo VG Scientific) equipped with a micro-focused monochromator X-ray source. The EA was performed in order to obtain the bulk compositions of the catalysts using a FlashEA 1112. The amounts of P and residual metals in the carbons were obtained *via* ICP analysis (POLY SCAN 61 E). The doping concentration of the dopants in the carbon was expressed using the atomic ratio of the dopant atoms to the carbon atoms measured *via* EA-ICP or XPS. The XRD patterns were acquired using a D/MAX-2500 (Rigaku) operated at 40 kV and 300 mA. The step–scan patterns were collected in the 20–80° (2θ ranges) range with a step size of 0.01° and scan speed of 1 deg min^{-1}. The data from the Raman spectroscopy were obtained using a Lab-RAM HR UV/Vis/NIR with a 514 nm Ar ion CW laser source. A BET surface area analysis was performed using a Micrometrics ASAP 2010 apparatus at 77 K. Prior to measurement, all samples were degassed and dehydrated at 200 °C for 2 h.

2.3 Electrochemical characterizations

The electrochemical properties of the prepared catalysts were analyzed using a three-electrode beaker cell equipped with a Pt wire counter-electrode (ALS Co. 002233), an Ag/AgCl reference electrode (ALS Co., 012167), and a rotating ring disk electrode (ALS Co. 011162), using an electrochemical analyzer (CHI700D, CH Instruments Inc.) and a rotator (RRDE-3A, ALS Co.). A commercial Pt/C (40 wt%) catalyst was purchased from E-tek in order to compare the electrochemical properties. The working electrodes were prepared using the thin film electrode method. The catalysts (10 mg) were dispersed in ink solution (1 mL; DI-water (15), 5 wt% Nafion in water (4), and isopropyl alcohol (1); the number in parenthesis indicates the volumetric ratio) followed by sonication. Then, the catalyst inks (5 μL) were dropped onto the glassy carbon of a rotating ring disk electrode (RRDE). The catalyst inks were dried at room temperature. 100 cycles of the cyclic voltammetry (CV) experiments were conducted in deaerated 1 M $HClO_4$ electrolyte in order to activate the catalysts with a 40 mV s^{-1} scan rate from −0.22 V to 1 V (*vs.* Ag/AgCl). The data from the last cycle were selected for the comparison of the CV results. The ORR experiments were conducted in an O_2 saturated 1 M $HClO_4$ electrolyte with a 5 mV s^{-1} scan rate and 2000 rpm rotating velocity from 0.82 V to −0.08 V (*vs.* Ag/AgCl). A constant potential (1.0 V, *vs.* Ag/AgCl) was applied to the Pt ring disk electrode during the ORR experiment. The following equation was used to calculate the yield of H_2O_2 formation:

$$H_2O_2\ (\%) = 200 \times \frac{I_R/N}{I_R/N + I_D} \quad (1)$$

where I_R and I_D are the currents at the ring and the disk, respectively, and N is the collection efficiency (0.37).

3. Results and discussion

3.1 Structural modifications by P-doping

Fig. 1 shows the morphologies of the prepared catalysts obtained from the TEM images. As shown in Fig. 1(a), the NDC formed a horn-type structure. However, the morphologies of the catalysts were altered after the P-doping. The TEM images of the PNDC-5 (Fig. 1(b)) and PNDC-10 (Fig. 1(c)) indicated tube-type

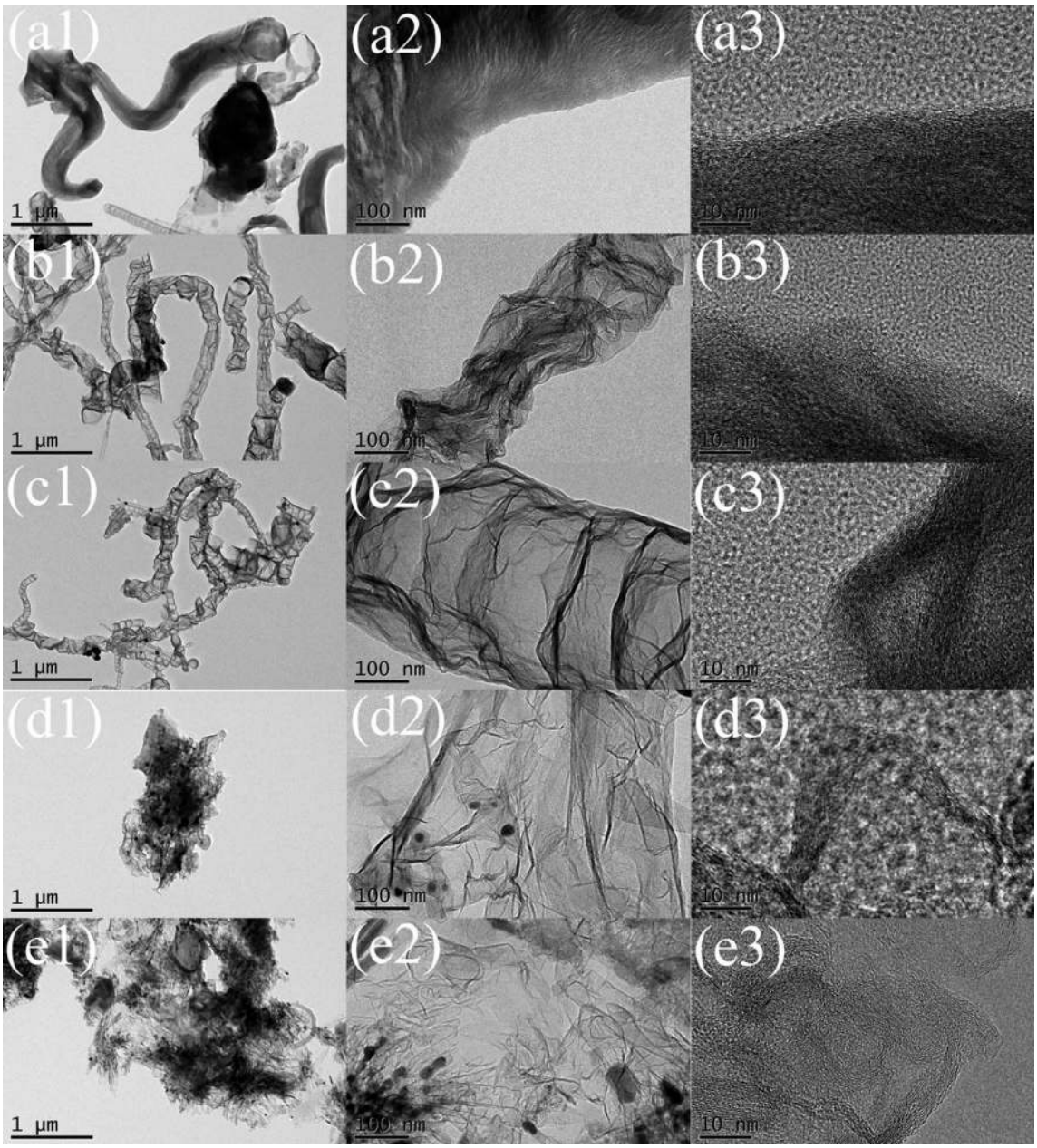

Fig. 1 TEM images of the prepared catalysts for (a) NDC, (b) PNDC-5, (c) PNDC-10, (d) PNDC-15, and (e) PNDC-20, and are indicated by 1 to 3 according to the magnifications (1. × 6000; 2. × 40 000; 3. × 400 000). "x3" images (x = a to e) are captured at the edge of the catalysts.

structures, but they differed with respect to the general CNTs reported.[32,33] The surfaces of the PNDC-5 and PNDC-10 were uneven and severely wrinkled as shown in Fig. 1(b) and (c), respectively. As the amount of P-doping increased, the structures of the PNDC-15 and PNDC-20 were altered to lump-type structures (Fig. 1(d) and (e), respectively). Furthermore, they exhibited an uneven surface; the catalyst was composed of crumpled carbon sheets with a thickness of approximately 5 nm. Moreover, the catalyst edges were also modified as the P was doped onto the NDC. The TEM images at the edge of the catalysts demonstrated that the even edged sites of the NDC (Fig. 1(a)) were transformed into open edge sites being split and angled (Fig. 1(b)–(e)), and the characteristics were intensified with increasing amounts of P-doping. Some metal residues remained and these are seen in the TEM images, even after iterative acid treatment with aqua regia. This occurred because some barriers, such as the carbon layers, covered the metal and prevented the dissolution in aqua regia.[34,35]

3.2 Compositions and doping concentrations

The surface compositions of the prepared catalysts were calculated from the XPS results (Table 1). The presence of P at the surface of the catalysts synthesized from the DCDA pyrolysis with phosphoric acid was confirmed. However, the P content at the surface of the catalysts for PNDC-5 and PNDC-10 had lower values than the detection limit (<1%); thus, an accurate P content is not calculable. As the amount of added phosphoric acid

Table 1 Surface compositions and doping concentrations of the prepared catalysts calculated from the XPS analysis

	Compositions[a]				Doping concentration[b]		
Catalysts	C	O	N	P	O/C	N/C	P/C
NDC	91.5	4.8	3.7	—	5.2	4.0	—
PNDC-5	90.8	5.2	3.0	<1.0	5.7	3.3	<1.0
PNDC-10	87.0	7.0	5.0	<1.0	8.0	5.7	<1.0
PNDC-15	84.5	9.1	5.0	1.4	10.8	5.9	1.7
PNDC-20	82.2	8.5	7.0	2.3	10.3	8.5	2.8

[a] at%. [b] Atomic ratio × 100.

increased, the P-doping concentrations at the surface also increased, up to 2.8%. Both the P-doping concentrations and the N-doping concentrations were increased from 4.0% for the NDC to 8.5% for the PNDC-20 with the increasing phosphoric acid additions. Therefore, it can be concluded that the addition of the phosphoric acid to the DCDA precursor composite assists nitrogen doping into carbon.

The bulk compositions of the prepared catalysts were obtained from the EA (N, C, and H) and ICP (P, Co, and Fe); the results are summarized with the calculated doping concentrations in Table 2. Similar to the surface composition from the XPS (Table 1), the N-doping concentration of the catalysts increased with increasing amounts of phosphoric acid added to the bulk. This also supports the results that the addition of phosphoric acid induced greater N-doping in the carbon. The P-doping amount also increased from 0.5 for PNDC-5 to 4.5 for PNDC-20, but these are much higher values compared with those at the surface (from <1 for PNDC-5 to 2.8 for PNDC-20). The reason for the difference in the P-doping amount can be found from the EDS experiments. Fig. 2 shows the EDS images of PNDC-20 that are mapped for C, P, Co, and Fe. The XPS results in Table 1 reveal that P is doped into the carbon at the catalyst surface, but P is not detected at the carbon position as seen in Fig. 2. This results from the low doping concentration of P onto the carbon surface, which is a lower value than the detection limit of the EDS. However, a vivid P detection emerges at the same position, where Co and Fe are also detected. Therefore, it can be understood that most P is bonded or doped with the metals rather than to the carbon. As mentioned above, the metal exposed to the surface of the catalysts is removed through iterative acid treatments. The residual metal is covered with a carbon barrier; therefore, the difference in the amount of P at the surface and at the bulk is created.

Table 2 Bulk compositions and doping concentrations of the prepared catalysts obtained from the EA and ICP analysis

	EA[a]			ICP[a]				
Catalysts	N	C	H	P	Co	Fe	N/C[b]	P/C[b]
NDC	3.3	82.8	0.1	0	1.9	0.7	3.4	0
PNDC-5	3.5	76.8	0.1	0.9	5.1	1.6	3.9	0.5
PNDC-10	4.1	66.7	0.3	3.0	10.3	3.0	5.3	1.7
PNDC-15	5.7	54.6	0.5	5.9	14.9	3.9	8.9	4.2
PNDC-20	4.3	49.7	0.8	5.8	11.8	6.0	7.4	4.5

[a] Compositions obtained from EA and ICP results (wt%). [b] Doping concentration (atomic ratio × 100).

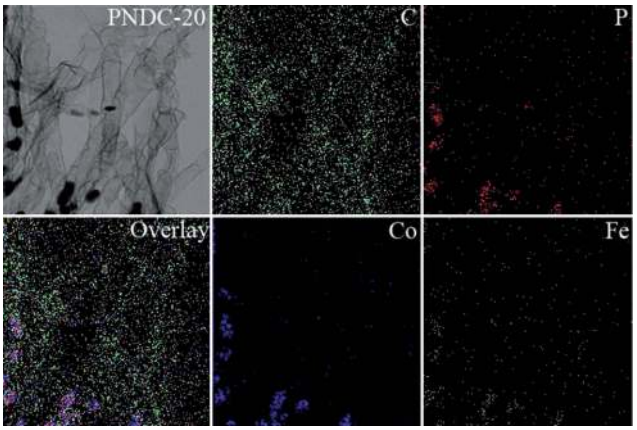

Fig. 2 EDS mapping images of PNDC-20.

3.3 Phases of the prepared catalysts

The XRD results (Fig. 3) indicate that the P and metals are present in the metal phosphide phase. The XRD data of the NDC exhibit peaks of the metallic Co (JCPDS 15-0806) and Fe (JCPDS 06-0696), which are the residual metals in the catalyst after the acid treatment. However, as the amount of added phosphoric acid increased (PNDC catalysts), the intensity of the metallic Co and Fe peaks gradually decreased; furthermore, new metal phosphide peaks appeared. These peaks were assigned to Co_2P (JCPDS 32-0306), but they were slightly shifted due to the incorporation of Fe into Co_2P. Because Co_2P is thermally stable (m.p. 1386 °C), it can stay without breaking the Co–P bonding after 900 °C of heat treatment. Furthermore, as shown in Fig. 4, the quantity of the residual metals increases as the amount of P increases. This demonstrates that the bonding of P with metals hinders the dissolution of the metals in acid.

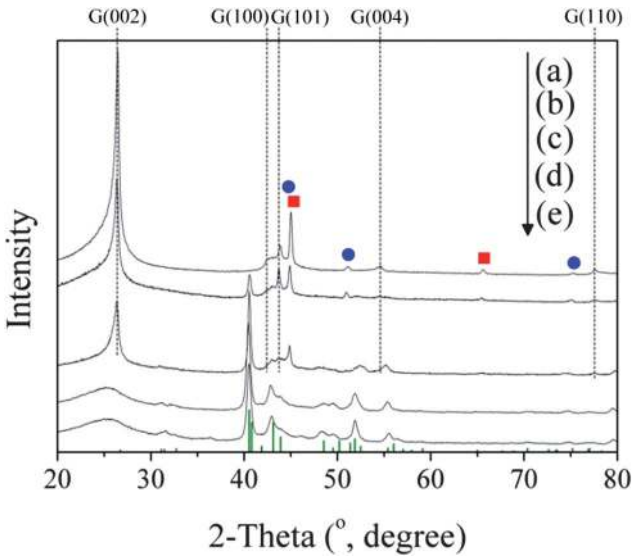

Fig. 3 XRD results of the prepared catalysts: (a) NDC, (b) PNDC-5, (c) PNDC-10, (d) PNDC-15, and (e) PNDC-20. The results are assigned for graphite (dotted line), Co (circle), Fe (rectangle), and Co_2P (bars beneath the graph).

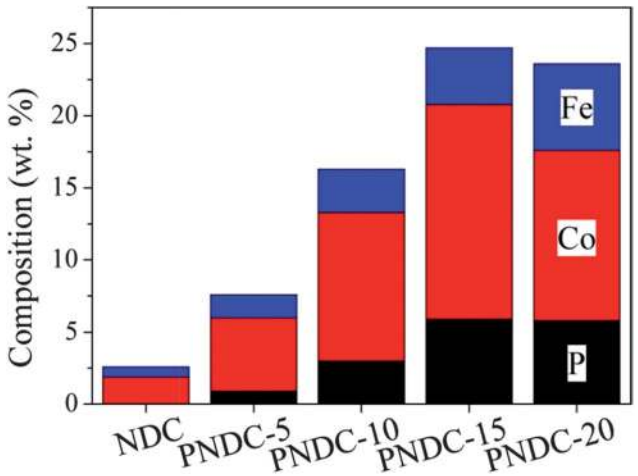

Fig. 4 The amount of residual P, Co, and Fe after the acid treatment obtained from ICP experiments.

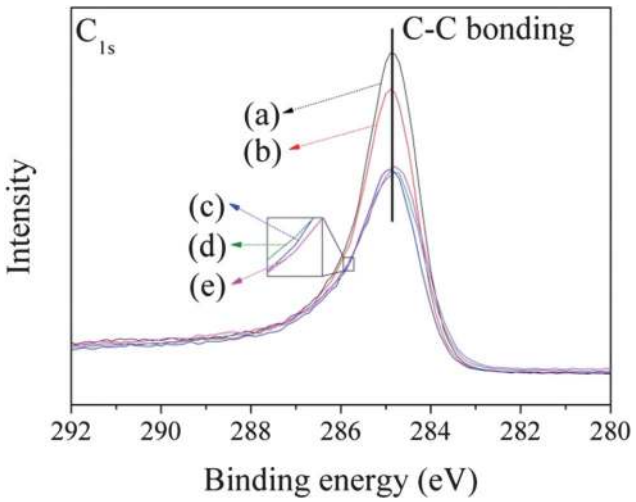

Fig. 5 XPS-C_{1s} data of the (a) NDC, (b) PNDC-5, (c) PNDC-10, (d) PNDC-15, and (e) PNDC-20. C–C bonding is indicated with solid line at 284.5 eV.

In the XRD results of the NDC (Fig. 3), a graphite peak (JCPDS 41-1487) in the (002) plane appeared distinguishably sharp and narrow; it was confirmed that the graphite structure was driven through the carbonization of the DCDA on the metal chlorides. However, peak intensity decrements were observed in PNDC-5 and PNDC-10; furthermore, the sharp peaks disappeared in PNDC-15 and PNDC-20. This result reveals that the addition of the phosphoric acid induces decrements in crystallinity for the NDC. As shown in Tables 1 and 2, the addition of phosphoric acid encouraged the doping of heteroatoms including N and P. Generally, the heteroatom doping in carbon induces defect sites and destruction in the carbon lattice, resulting in low crystallinity. In particular, the structural corruption by P-doping will be more effective than that by N-doping because P has a much larger covalent radius (107 ± 3 pm) than that of C (73 pm) or N (71 ± 1 pm).

3.4 Deformation of the graphitic structure

The deformation of the carbon structure due to the heteroatom doping was also supported by the experimental results of the XPS-C_{1s} (Fig. 5) and Raman spectroscopy (Fig. 6). In the XPS-C_{1s} results, the C–C bonding peak resulting from the sp^2-bonding between the carbon atoms was found at 284.5 eV.[36] All prepared catalysts exhibited a peak at 284.5 eV as shown in Fig. 5. However, the peak intensities declined and broadened as the amount of doping increased. This reveals that the degree of sp^2-bonding of the carbon lowered with the heteroatom doping. Moreover, the Raman spectroscopy results further confirm the conclusion derived from the XRD and XPS-C_{1s} results. In the Raman spectroscopy of all sp^2-carbons, two conspicuous peaks emerged at approximately 1580 cm^{-1} of the G-band and 1352 cm^{-1} of the D-band. The G-band peak results from the E_{2g} vibrational mode in the D^4_{6h} symmetry group of the graphite crystal planes. The D-band originates from the lattice distortion in the sp^2-hybridized carbon and becomes active due to the presence of various defects (*e.g.* vacancy, topological defects, impurities, *etc.*). Therefore, the ratio of intensities for the D-band and G-band (I_D/I_G) is commonly used as a value for the degree of

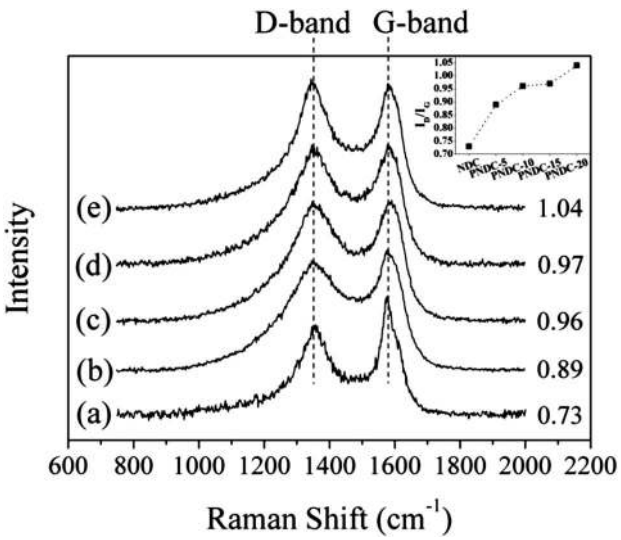

Fig. 6 The D-band and G-band in Raman spectroscopy for the prepared catalysts: (a) NDC, (b) PNDC-5, (c) PNDC-10, (d) PNDC-15, and (e) PNDC-20. The ratio of D-band to G-band (I_D/I_G) is indicated in each result and graphed in the figure.

defect of the carbon.[37] As shown in Fig. 6, the I_D/I_G of the prepared catalysts increased from 0.73 for NDC to 1.04 for PNDC-20 by increasing amounts of doping. This indicates that the heteroatom doping in the carbon develops defect sites, and it coincides with the results from the XRD and XPS-C_{1s}.

3.5 Surface area and doping types (N and P)

The additional doping of P into NDC also changes the surface area and pore size of the catalysts (Fig. 7). The NDC exhibits 108.1 $m^2\ g^{-1}$ of BET surface area, but after additional P-doping, the area increases to 207.8, 240.2, 234.2, and 578.5 $m^2\ g^{-1}$ for the PNDC-5, PNDC-10, PNDC-15, and PNDC-20, respectively, even though the PNDCs include more metal residue (Fig. 4). If it

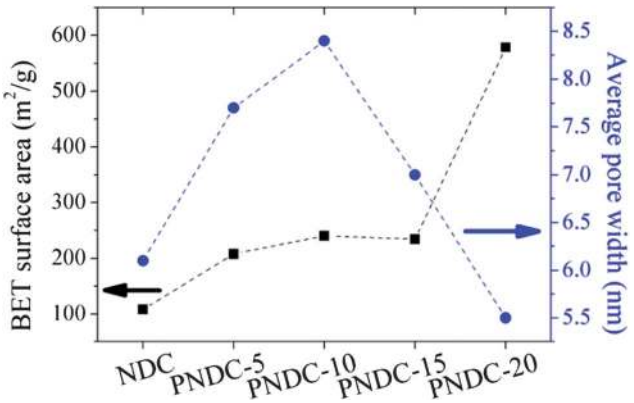

Fig. 7 BET surface areas and average pore widths of the prepared catalysts.

is assumed that the surface area of the catalyst is an effect of the carbon only, the carbon normalized BET areas of the catalysts are 130.6, 270.6, 360.1, 428.9, and 1164.0 $m^2\ g^{-1}$ for the NDC, PNDC-5, PNDC-10, PNDC-15, and PNDC-20, respectively. The PNDC-20 has a surface area that is almost nine times higher than that of the NDC. The average pore width is 6.1 nm for the NDC, but it increases to 7.7 and 8.4 nm for the PNDC-5 and PNDC-10, respectively, and decreases to 7.0 and 5.5 nm for PNDC-15 and PNDC-20, respectively. As mentioned above, phosphoric acid is one of many widely used activating agents for carbon activation: it burns the carbon surface and results in the production of many pores and increases the surface area.[29–31] Moreover, as shown in the TEM images (Fig. 1), the addition of phosphoric acid changes the morphology of the carbon from a horn-type structure with an even surface in the NDC to tube-type and lump-type structures with uneven surfaces in the PNDCs according to the increase of the P-doping. Therefore, it can be concluded that the activation of the NDC *via* phosphoric acid and/or morphological refinement would increase the surface area of the catalysts.

Table 3 Doping types and proportions of N and P in the catalysts

	N[a]			P[b]		
Catalysts	N1	N2	N3	P1	P2	P3
NDC	48.7	46.3	5.0	—	—	—
PNDC-5	48.4	46	5.6	44	46.3	9.7
PNDC-10	49.4	45.1	5.5	49.6	45.0	5.4
PNDC-15	49.3	44.3	6.4	28.8	63.3	7.9
PNDC-20	46.8	48.5	4.7	43.6	51.0	5.4

[a] N1 = pyridinic-N, N2 = pyrrolic- or graphitic-N, and N3 = pyridinic-oxide. [b] P1 = Me_xP (Me = Co or Fe; x = 1–2), P2 = P–O, and P3 = P–C.

The doping type of the N and P doped in the carbon was investigated through XPS analysis, as shown in Fig. 8. N is doped as pyridinic-N (N1), pyrrolic-N or graphitic-N (N2), and pyridinic oxide (N3): the XPS-N_{1s} result is deconvoluted according to each peak.[35,38] P is doped as Me_xP (Me = Co or Fe; x = 1–2; P1), P–O (P2), and P–C (P3): the XPS-P_{2p} result is deconvoluted according to these peaks.[39–41] The results are organized numerically in Table 3. In the XPS-N_{1s}, the results exhibit similar shapes regardless of the amount of phosphoric acid included. N1 and N2 are the dominant doping phases in the prepared catalysts and their proportions range from 46.8 to 49.4% and from 44.3 to 48.5%, respectively, regardless of the amount of phosphoric acid added. This reveals that the proportion of N-doping types is not significantly affected by the presence of phosphoric acid. Likewise, the XPS-P_{2p} result exhibited similar proportions of the P-doping types (28.8 to 49.6% for P1, 45.0 to 63.6% for P2, and 5.4 to 9.7% for P3) even though the intensity of the peaks increase as the P-doping increases, which indicates that P2 is a dominant phase of the P-doping. In Table 1, the surface composition analysis reveals that the oxygen content of the catalysts increases as the P-doping increases. P2 (P–O) is the dominant phase in the P-doping; therefore, it can be derived that increasing the P-doping bonded with oxygen results in the increase of the oxygen content at the surface of the catalysts.

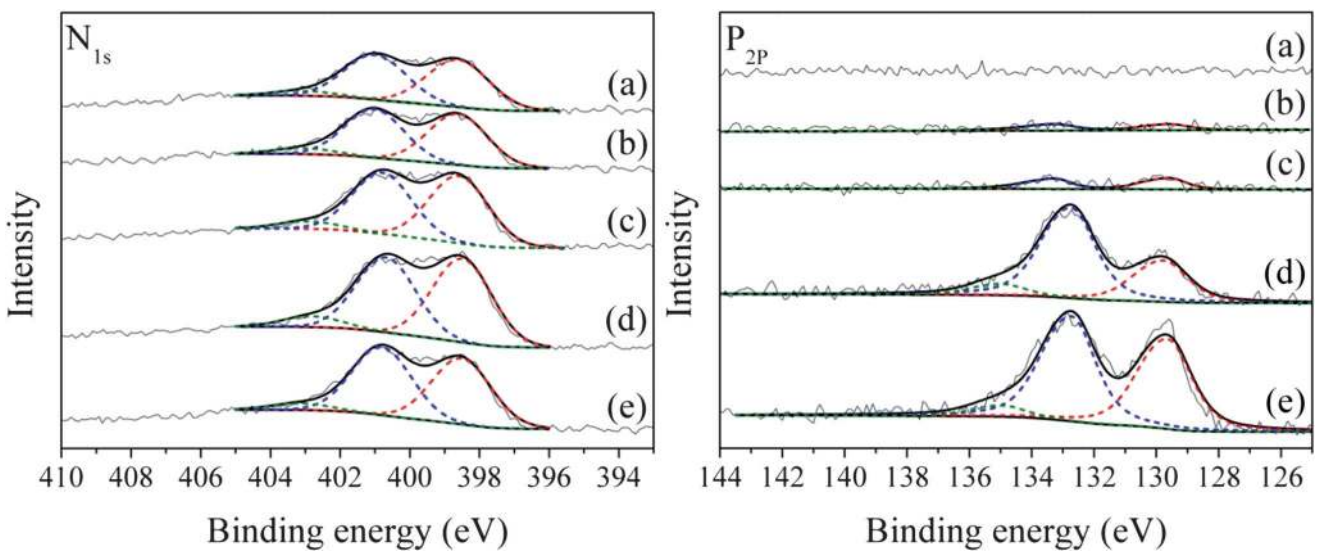

Fig. 8 (left) XPS-N_{1s} and (right) -P_{2p} results of (a) NDC, (b) PNDC-5, (c) PNDC-10, (d) PNDC-15, and (e) PNDC-20. Each peak is deconvoluted to pyridinic-N (red), pyrrolic-N or graphitic-N (blue), and pyridinic oxide (green) in XPS-N_{1s} analysis, and to Me_xP (Me = Co or Fe; x = 1–2; red), P–O (blue), and P–C (green) in XPS-P_{2p}.

3.6 Cyclic voltammetry and capacitance

Fig. 9 shows the CV results of the prepared catalysts in deaerated 1 M $HClO_4$. The CV data do not present unique peaks and the results are similar to the CV results of graphite.[42] The CV area is closely related to the capacitance of a given material.[16] In Fig. 9, the CV area of the NDC recorded the lowest value among the catalysts. However, after P-doping, the CV area increased (PNDC-5) and exhibited similar values for those of PNDC-10, PNDC-15 and PNDC-20. This means that the capacitance of NDC is modified by the additional P-doping; however, there is no other significant enhancement over PNDC-10. The capacitance is defined using the following equation;

$$C = \varepsilon \frac{A}{d} \quad (2)$$

where ε is the electrolyte dielectric constant, A is the surface area accessible to ions, and d is the distance between the center of the ion and carbon surface. This equation reveals that the capacitance is proportional to the surface area of the carbon. Therefore, it can be concluded that the enhanced capacitance *via* P-doping results from the increase in the surface area as shown in Fig. 7. However, additional P-doping induces defect sites and destroys the sp^2-carbon network in the carbon structure; this phenomenon become intensified with increasing levels of P-doping, as shown in Fig. 3, 5, and 6. It is well known that these factors, including the defects in the carbon and the destruction of the sp^2-carbon network, reduce the electrical conductivity of the carbon.[43–45] Therefore, it is considered that further increases in the capacitance are not obtained in the samples higher than PNDC-10 due to the diminished electrical conductivity of the prepared catalysts, even though the surface area of the catalysts is enlarged.

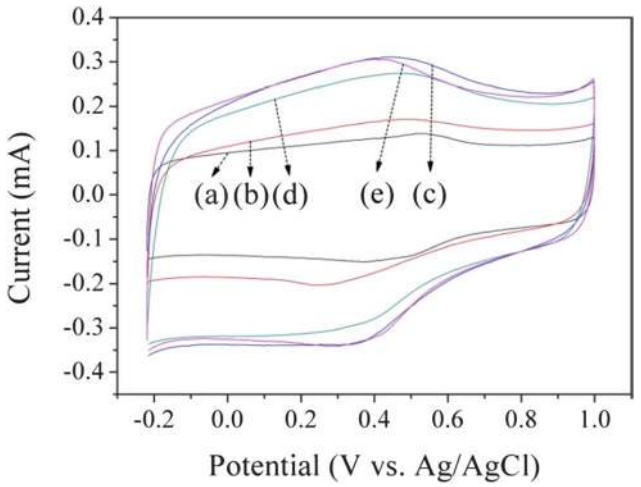

Fig. 9 CV results of (a) NDC, (b) PNDC-5, (c) PNDC-10, (d) PNDC-15, and (e) PNDC-20 in deaerated 1 M $HClO_4$.

3.7 Modifications in ORR activity and pathway by P-doping

The ORR activities of the catalysts were examined and are shown in Fig. 10. The NDC exhibits an onset potential at approximately 0.55 V (*vs.* Ag/AgCl), but the PNDCs reveal a slightly up-shifted onset potential near 0.6 V (*vs.* Ag/AgCl). The ORR activities of the prepared catalysts were compared at the kinetic region, 0.5 V (*vs.* Ag/AgCl), and the results are listed in Table 4, including the results of the Pt/C. The mass activity of the NDC is −0.69 mA mg^{-1} at 0.5 V (*vs.* Ag/AgCl), but the ORR activity of the catalyst was only promoted after the additional P-doping. The ORR activities decrease in the order of PNDC-10 > PNDC-15 > PNDC-20 > PNDC-5 > NDC. The ORR activity increases with the addition of P-doping up to PNDC-10; however, it decreases slightly with further P-doping (PNDC-15 and PNDC-20). The catalyst achieving the best ORR activity is the PNDC-10 with an activity of −2.88 mA mg^{-1}, which is more than fourfold that of NDC; it is approximately 31% of the ORR activity compared with that of commercial 40 wt% Pt/C (−9.22 mA mg^{-1}) at 0.5 V (*vs.* Ag/AgCl).

Both the ORR activity and ORR pathway were modified to a four-electron pathway. In the ORR, the oxygen is reduced to two different pathways: a two-electron pathway producing H_2O_2

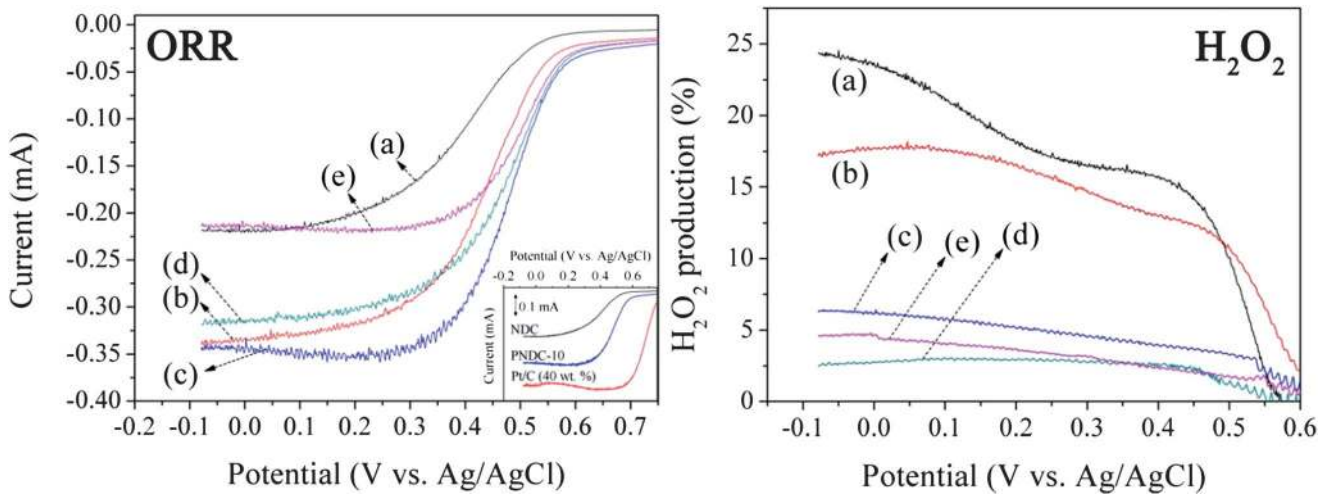

Fig. 10 ORR activities in O_2 saturated 1 M $HClO_4$ (left), and calculated H_2O_2 production yields (right) of the prepared catalysts during the ORR: (a) NDC, (b) PNDC-5, (c) PNDC-10, (d) PNDC-15, and (e) PNDC-20. ORR activity of the commercial Pt/C (40 wt%) is compared with those of the NDC and PNDC-10, and illustrated in the figure.

Table 4 Electrochemical results of the prepared catalysts obtained at 0.5 V (*vs.* Ag/AgCl)

Catalysts	Current[a]	M.A.[b]	H_2O_2 (%)[c]
NDC	−0.034	−0.69	10.1
PNDC-5	−0.087	−1.74	10.7
PNDC-10	−0.144	−2.88	3.3
PNDC-15	−0.129	−2.57	1.3
PNDC-20	−0.116	−2.32	1.6
Pt/C	−0.461	−9.22	0.8

[a] Oxygen reduction activity (mA). [b] Mass activity (mA mg^{-1}). [c] H_2O_2 production yield (%).

and a four-electron pathway producing H_2O.[46] The H_2O_2 produced in the two-electron pathway causes degradation of the membrane and catalyst resulting in declining cell performance in the PEMFCs.[47] Therefore, the four-electron pathway is desirable in the ORR. As shown in Fig. 10, the H_2O_2 production yield during the ORR is calculated from the disk and Pt-ring disk currents of the RRDE. The NDC exhibits a high H_2O_2 production yield during the ORR; however, this is diminished *via* additional P-doping. The H_2O_2 production yields of the catalysts are compared at 0.5 V (*vs.* Ag/AgCl) and shown in Table 4. The H_2O_2 production yield of NDC is 10.1%; however, this value was reduced exponentially with additional P-doping: 10.7% for PNDC-5 and below 4% for PNDC-10, PNDC-15, and PNDC-20. Therefore, it can be concluded that the additional P-doping modifies both the ORR activity and pathway for NDC in acidic media.

3.8 Active sites and effects of P-doping on ORR activity

Numerous studies on heteroatom-doped carbon for the ORR catalysts have been undertaken over the past decade, and many factors determining the ORR activity of the catalysts have been proposed. One suggested active site is the Me–N_x complex.[48–50] However, it was revealed that this bonding is destroyed at high temperatures (>800 °C),[51,52] and all prepared samples (NDC and PNDCs) are pyrolyzed at 900 °C. In the PNDCs, the presence of the MeP_x phase was demonstrated through XRD and XPS analyses, but most of the phase at the PNDC surface is eliminated through acid treatments with aqua regia. Although residual MeP_x is present after the acid treatment, the complex is covered and protected by thin barriers (*e.g.* carbon layer) and cannot participate in the ORR which occurs on the catalyst surfaces.[34,35] Therefore, it is concluded that the metal complex is not crucial in the enhancement of the ORR activity for PNDCs. In addition, it was revealed that the pyridinic-N site is the most active site in the ORR among all types of N-doping.[15,53] However, as shown in Fig. 8, the additional P-doping does not change the distribution of the N-doping type, and all catalysts exhibit similar proportions ranging from 46.8 to 49.4%.

It is suggested that important determinants for improved ORR activity *via* additional P-doping are the morphological modifications. It has been revealed both experimentally and theoretically that the edge sites are more active toward ORR than the facets of the heteroatom doped carbon.[53–55] As shown in the TEM images (Fig. 1), additional P-doping induces uneven and wrinkled surfaces with the open edge sites becoming split and angled. Moreover, surface area expansion resulting from the P-doping (Fig. 7) has positive effects on the ORR activity of the catalysts, as the ORR is a surface reaction and the large surface area of the catalysts provides many active sites. Increasing the doping concentration of both N and P, or the presence of P, could provide a rationale for the activity improvement of NDC. It has been proposed that the doping of N into carbon allows charge delocalization and results in a slightly positive charge of carbon atoms adjacent to the doped N atom due to the high electron negativity of N.[17,56] Thus, the positively charged carbon atoms acts as an active site for the ORR through the provision of adsorption sites of oxygen molecules. Moreover, the asymmetric spin density introduced by the heteroatom doping into carbon offers active sites for the ORR.[56] It has been reported that the doping of other heteroatoms excluding N also encourages asymmetry in the spin density and enhances the ORR activity of carbon.[57] Therefore, it is concluded that increasing N- or P-doping concentrations (Table 1), or the presence of P, can enhance the charge delocalization or asymmetric spin density, thus promoting catalytic activity of the catalysts toward the ORR. However, it remains unclear as to which factor is the crucial factor determining the ORR activity enhancement of the prepared catalysts; thus, further study is required.

As shown in Fig. 10, the ORR activity (at 0.5 V, *vs.* Ag/AgCl) of the NDC (−0.69 mA mg^{-1}) increases through additional P-doping up to PNDC-5 (−1.74 mA mg^{-1}) and PNDC-10 (−2.88 mA mg^{-1}), but decreases slightly with further addition of P-doping (−2.57 and −2.32 mA mg^{-1} for PNDC-15 and PNDC-20, respectively). The ORR occurs at the three-phase boundary (TPB) where the oxygen, proton, and electron meet. However, the high doping of the heteroatoms in the carbon introduces many defect sites, which decreases the degree of sp^2-carbon network, as shown in Fig. 3, 5, and 6. The destroyed carbon structure is unable to provide an effective electron path, thus decreasing the electrical conductivity.[43–45] Therefore, effective TPB formation is hindered due to the resistance of the electron transport and this lowers the catalytic activity of the PNDCs towards the ORR after PNDC-10.

4. Conclusions

As a new strategy for developing ORR activity for carbon-based catalysts, the dual doping of both P and N into carbon was attempted and its physical and electrochemical characteristics in acidic media were investigated. The P, N-doped carbon was prepared *via* pyrolysis of the DCDA and phosphoric acid onto $CoCl_2$ and $FeCl_2$. The DCDA and phosphoric acid were used as the sources of C–N and P, respectively; the amount of P-doping was controlled by changing the amount of phosphoric acid added. The TEM study revealed that additional P-doping modifies the morphology of the catalysts to uneven surfaces with the open edge sites being split and angled, and it increases the surface area of the catalysts. Moreover, it was confirmed that the increment of the additional phosphoric acid facilitates doping for all heteroatoms (*i.e.* N, P, and O), but results in the structural collapse of the carbon network. In the ORR, additional P-doping promotes the catalytic activity of NDC and an optimized PNDC exhibits more than fourfold increase in mass activity compared with that of the NDC. However, further doping of P over

PNDC-10 lowered the ORR activity due to the destruction of the carbon network. In this study, the morphological modification, surface area expansion, and increased doping concentration of N–P (or P-doping itself) are proposed as the cause for the improvement in the ORR activity of the catalysts.

Acknowledgements

This work was supported by the National Research Foundation of Korea (NRF) grant funded by the Korean government (MEST) (no. 2011-0029812).

Notes and references

1 R. Borup, J. Meyers, B. Pivovar, Y. S. Kim, R. Mukundan, N. Garland, D. Myers, M. Wilson, F. Garzon, D. Wood, P. Zelenay, K. More, K. Stroh, T. Zawodzinski, J. Boncella, J. E. McGrath, M. Inaba, K. Miyatake, M. Hori, K. Ota, Z. Ogumi, S. Miyata, A. Nishikata, Z. Siroma, Y. Uchimoto, K. Yasuda, K. I. Kimijima and N. Iwashita, *Chem. Rev.*, 2007, **107**, 3904–3951.
2 K. Sopian and W. R. W. Daud, *Renewable Energy*, 2006, **31**, 719–727.
3 X. W. Yu and S. Y. Ye, *J. Power Sources*, 2007, **172**, 133–144.
4 Y. Y. Shao, G. P. Yin and Y. Z. Gao, *J. Power Sources*, 2007, **171**, 558–566.
5 X. F. Yang, J. Hu, J. Fu, R. Q. Wu and B. E. Koel, *Angew. Chem., Int. Ed.*, 2011, **50**, 10182–10185.
6 J. L. Fernandez, D. A. Walsh and A. J. Bard, *J. Am. Chem. Soc.*, 2005, **127**, 357–365.
7 M. Neergat, V. Gunasekar and R. Rahul, *J. Electroanal. Chem.*, 2011, **658**, 25–32.
8 Z. W. Chen, D. Higgins, A. P. Yu, L. Zhang and J. J. Zhang, *Energy Environ. Sci.*, 2011, **4**, 3167–3192.
9 D. G. Xia, S. Z. Liu, Z. Y. Wang, G. Chen, L. J. Zhang, L. Zhang, S. Q. Hui and J. J. Zhang, *J. Power Sources*, 2008, **177**, 296–302.
10 X. X. Yuan, X. Zeng, H. J. Zhang, Z. F. Ma and C. Y. Wang, *J. Am. Chem. Soc.*, 2010, **132**, 1754–1755.
11 M. S. Thorum, J. Yadav and A. A. Gewirth, *Angew. Chem., Int. Ed.*, 2009, **48**, 165–167.
12 P. H. C. Camargo, Z. M. Peng, X. M. Lu, H. Yang and Y. N. Xia, *J. Mater. Chem.*, 2009, **19**, 1024–1030.
13 H. S. Oh, J. G. Oh, B. Roh, I. Hwang and H. Kim, *Electrochem. Commun.*, 2011, **13**, 879–881.
14 W. Xiong, F. Du, Y. Liu, A. Perez, M. Supp, T. S. Ramakrishnan, L. M. Dai and L. Jiang, *J. Am. Chem. Soc.*, 2010, **132**, 15839–15841.
15 N. P. Subramanian, X. G. Li, V. Nallathambi, S. P. Kumaraguru, H. Colon-Mercado, G. Wu, J. W. Lee and B. N. Popov, *J. Power Sources*, 2009, **188**, 38–44.
16 K. R. Lee, K. U. Lee, J. W. Lee, B. T. Ahn and S. I. Woo, *Electrochem. Commun.*, 2010, **12**, 1052–1055.
17 K. P. Gong, F. Du, Z. H. Xia, M. Durstock and L. M. Dai, *Science*, 2009, **323**, 760–764.
18 S. Y. Wang, D. S. Yu, L. M. Dai, D. W. Chang and J. B. Baek, *ACS Nano*, 2011, **5**, 6202–6209.
19 D. S. Geng, Y. Chen, Y. G. Chen, Y. L. Li, R. Y. Li, X. L. Sun, S. Y. Ye and S. Knights, *Energy Environ. Sci.*, 2011, **4**, 760–764.
20 Z. Q. Luo, S. H. Lim, Z. Q. Tian, J. Z. Shang, L. F. Lai, B. MacDonald, C. Fu, Z. X. Shen, T. Yu and J. Y. Lin, *J. Mater. Chem.*, 2011, **21**, 8038–8044.
21 Y. Zheng, Y. Jiao, J. Chen, J. Liu, J. Liang, A. Du, W. M. Zhang, Z. H. Zhu, S. C. Smith, M. Jaroniec, G. Q. Lu and S. Z. Qiao, *J. Am. Chem. Soc.*, 2011, **133**, 20116–20119.
22 G. Wu, K. L. More, C. M. Johnston and P. Zelenay, *Science*, 2011, **332**, 443–447.
23 G. Liu, X. G. Li, J. W. Lee and B. N. Popov, *Catal. Sci. Technol.*, 2011, **1**, 207–217.
24 G. Liu, X. G. Li, P. Ganesan and B. N. Popov, *Electrochim. Acta*, 2010, **55**, 2853–2858.
25 M. Lefevre, E. Proietti, F. Jaouen and J. P. Dodelet, *Science*, 2009, **324**, 71–74.
26 J. Ozaki, N. Kimura, T. Anahara and A. Oya, *Carbon*, 2007, **45**, 1847–1853.
27 C. H. Choi, S. H. Park and S. I. Woo, *Green Chem.*, 2011, **13**, 406–412.
28 Z. W. Liu, F. Peng, H. J. Wang, H. Yu, W. X. Zheng and J. A. Yang, *Angew. Chem., Int. Ed.*, 2011, **50**, 3257–3261.
29 M. Molinasabio, F. Rodriguezreinoso, F. Caturla and M. J. Selles, *Carbon*, 1995, **33**, 1105–1113.
30 A. M. Puziy, O. I. Poddubnaya, A. Martinez-Alonso, F. Suarez-Garcia and J. M. D. Tascon, *Appl. Surf. Sci.*, 2002, **200**, 196–202.
31 A. M. Puziy, O. I. Poddubnaya, R. P. Socha, J. Gurgul and M. Wisniewski, *Carbon*, 2008, **46**, 2113–2123.
32 A. V. Okotrub, L. G. Bulusheva, A. G. Kudashov, V. V. Belavin, D. V. Vyalikh and S. L. Molodtsov, *Appl. Phys. A: Mater. Sci. Process.*, 2009, **94**, 437–443.
33 R. H. Baughman, A. A. Zakhidov and W. A. de Heer, *Science*, 2002, **297**, 787–792.
34 C. H. Choi, S. Y. Lee, S. H. Park and S. I. Woo, *Appl. Catal., B*, 2011, **103**, 362–368.
35 C. H. Choi, S. H. Park and S. I. Woo, *Int. J. Hydrogen Energy*, 2012, **37**, 4563–4570.
36 G. Nanse, E. Papirer, P. Fioux, F. Moguet and A. Tressaud, *Carbon*, 1997, **35**, 175–194.
37 K. Ghosh, M. Kumar, T. Maruyama and Y. Ando, *Carbon*, 2009, **47**, 1565–1575.
38 P. H. Matter, L. Zhang and U. S. Ozkan, *J. Catal.*, 2006, **239**, 83–96.
39 P. E. R. Blanchard, A. P. Grosvenor, R. G. Cavell and A. Mar, *Chem. Mater.*, 2008, **20**, 7081–7088.
40 F. Claeyssens, G. M. Fuge, N. L. Allan, P. W. May and M. N. R. Ashfold, *Dalton Trans.*, 2004, 3085–3092.
41 O. S. Panwar, M. A. Khan, M. Kumar, S. M. Shivaprasad, B. S. Satyanarayana, P. N. Dixit and R. Bhattacharyya, *Jpn. J. Appl. Phys.*, 2009, **48**, 065501.
42 J. H. Chen, W. Z. Li, D. Z. Wang, S. X. Yang, J. G. Wen and Z. F. Ren, *Carbon*, 2002, **40**, 1193–1197.
43 H. S. Myung, Y. S. Park, B. Hong, J. G. Han, Y. H. Kim, J. Y. Lee and L. R. Shaginyan, *Thin Solid Films*, 2006, **494**, 123–127.
44 Z. R. Ismagilov, A. E. Shalagina, O. Y. Podyacheva, A. V. Ischenko, L. S. Kibis, A. I. Boronin, Y. A. Chesalov, D. I. Kochubey, A. I. Romanenko, O. B. Anikeeva, T. I. Buryakov and E. N. Tkachev, *Carbon*, 2009, **47**, 1922–1929.
45 H. Niwa, M. Kobayashi, K. Horiba, Y. Harada, M. Oshima, K. Terakura, T. Ikeda, Y. Koshigoe, J.-i. Ozaki, S. Miyata, S. Ueda, Y. Yamashita, H. Yoshikawa and K. Kobayashi, *J. Power Sources*, 2011, **196**, 1006–1011.
46 R. A. Sidik, A. B. Anderson, N. P. Subramanian, S. P. Kumaraguru and B. N. Popov, *J. Phys. Chem. B*, 2006, **110**, 1787–1793.
47 J. Wu, X. Z. Yuan, J. J. Martin, H. Wang, J. Zhang, J. Shen, S. Wu and W. Merida, *J. Power Sources*, 2008, **184**, 104–119.
48 R. Bashyam and P. Zelenay, *Nature*, 2006, **443**, 63–66.
49 S.-i. Yamazaki, Y. Yamada, T. Ioroi, N. Fujiwara, Z. Siroma, K. Yasuda and Y. Miyazaki, *J. Electroanal. Chem.*, 2005, **576**, 253–259.
50 L. C. Wang, L. Zhang and J. J. Zhang, *Electrochim. Acta*, 2011, **56**, 5488–5492.
51 E. Yeager, *Electrochim. Acta*, 1984, **29**, 1527–1537.
52 K. Wiesener, *Electrochim. Acta*, 1986, **31**, 1073–1078.
53 H. S. Oh, J. G. Oh, W. H. Lee, H. J. Kim and H. Kim, *Int. J. Hydrogen Energy*, 2011, **36**, 8181–8186.
54 T. Ikeda, M. Boero, S. F. Huang, K. Terakura, M. Oshima and J. Ozaki, *J. Phys. Chem. C*, 2008, **112**, 14706–14709.
55 H. Kim, K. Lee, S. I. Woo and Y. Jung, *Phys. Chem. Chem. Phys.*, 2011, **13**, 17505–17510.
56 L. P. Zhang and Z. H. Xia, *J. Phys. Chem. C*, 2011, **115**, 11170–11176.
57 Z. Yang, Z. Yao, G. Li, G. Fang, H. Nie, Z. Liu, X. Zhou, X. a. Chen and S. Huang, *ACS Nano*, 2011, **6**, 205–211.